Research Article Vol. 35, No. 5 / May 2018 / Journal of the Optical Society of America B A103

Journal of the Optical Society of America B OPTICAL PHYSICS

Single-cycle attosecond pulses by Thomson backscattering of terahertz pulses

György Tóth,[1,2,*] Zoltán Tibai,[1] Ashutosh Sharma,[3] József A. Fülöp,[2,3,4] and János Hebling[1,2,4]

[1]Institute of Physics, University of Pécs, 7624 Pécs, Hungary
[2]MTA-PTE High-Field Terahertz Research Group, 7624 Pécs, Hungary
[3]ELI-ALPS, ELI-Hu Nkft., 6720 Szeged, Hungary
[4]Szentágothai Research Centre, University of Pécs, 7624 Pécs, Hungary
*Corresponding author: tothgy@fizika.ttk.pte.hu

Received 1 November 2017; revised 23 March 2018; accepted 27 March 2018; posted 28 March 2018 (Doc. ID 312518); published 12 April 2018

The generation of single-cycle attosecond pulses based on Thomson scattering of terahertz (THz) pulses is proposed. In the scheme, a high-quality relativistic electron beam, produced by a laser-plasma wakefield accelerator, is sent through suitable magnetic devices to produce ultrathin electron layers for coherent Thomson backscattering of intense THz pulses. According to numerical simulations, single-cycle attosecond pulse generation is possible with up to 1 nJ energy. The waveform of the attosecond pulses closely resembles that of the THz pulses. This allows for flexible waveform control of attosecond pulses.

OCIS codes: (340.7480) X-rays, soft x-rays, extreme ultraviolet (EUV); (260.7120) Ultrafast phenomena; (280.1350) Backscattering; (320.5540) Pulse shaping.

https://doi.org/10.1364/JOSAB.35.00A103

1. INTRODUCTION

Attosecond pulses can be generated in a number of ways, such as high-harmonic generation [1], undulator radiation [2–5], or Thomson scattering [6–9]. High-harmonic generation is capable of producing single-cycle attosecond pulses [10]. Even subcycle pulses were generated by laser-generated ultrathin electron layers from double-foil targets [11]. However, controlling the pulse shape has not been demonstrated so far. This is also true of radiation sources based on relativistic electrons [5,12]. In order to circumvent this limitation, we proposed a technique to generate carrier-envelope phase stable, waveform-controlled single-cycle [13,14] or few-cycle [15] attosecond pulses by coherent undulator radiation. In this scheme, ultrathin (of a few nanometers) relativistic electron layers, generated in a laser-assisted bunching process, emit attosecond pulses when passing through a radiator undulator. The magnetic field distribution of the undulator is transferred to the waveform of the emitted radiation [13–15], thereby offering a unique waveform tailoring capability. Nevertheless, this technique requires high-energy (GeV) electrons, as an extremely short undulator would be necessary for lower-energy (<100 MeV) electrons, which are more easily available even from laser electron accelerators.

Laser-plasma-based electron acceleration [16–25], mediated by wake field, is able to generate electrons of GeV energy over acceleration distances of a few centimeters with parameters comparable to (and in some regards even better than) conventional sources. The pulse duration unique to laser-plasma wakefield accelerators (LPWAs) is intrinsically ultrashort (<30 fs), which can be more than one order of magnitude shorter than usual in x-ray free-electron lasers (XFELs). The recent progress in LPWAs [26] allows the efficient production of high-quality electron beams [17,18] in very high electric fields. Moreover, it has opened the possibility to conceive and design the compact setup of Ref. [27].

Alternatively, Thomson scattering is capable to generate attosecond pulses from low-energy electrons (see, e.g., [7]). Single-cycle attosecond pulse generation by Thomson scattering is possible using single-cycle laser pulses. However, single-cycle laser pulse generation is a big challenge in the visible spectral range. Therefore, alternative methods can be of significant interest.

In this paper, we propose a setup to generate waveform-controlled single-cycle attosecond pulses by Thomson scattering of intense terahertz (THz) pulses. In the THz spectral range, single-cycle pulse generation is straightforward [28–32]. The peak electric field of the so far most intense THz pulses generated by optical rectification reaches 40 MV/cm [30], and there are many suggestions to increase the efficiency of THz generation [33–38]. Here, we show that such THz pulses are a useful tool in generating single-cycle or waveform-controlled attosecond pulses by Thomson scattering on 30–40 MeV electrons, conveniently delivered by present laser-driven electron sources.

The paper is organized as follows. Section 2 describes the basics of Thomson scattering. Section 3 introduces the setup proposed in this work. Section 4 describes the calculation method. The results and their discussion are presented in Section 5. The conclusion is drawn in the last section.

2. SCHEME OF THE ATTOSECOND SOURCE

In order to generate attosecond pulses in the ultraviolet spectral range by Thomson scattering, ultrathin electron bunches are necessary. Efficient generation of radiation is possible only if the electron bunch length is shorter than half of the generated radiation wavelength. Few-nanometer-long electron layers (nanobunches) can be produced within the electron bunch for a short time, as described in our previous work [13,14]. In the scheme investigated here, the THz pulse is scattered on these nanobunches and generates attosecond pulses.

The proposed setup for the generation of single-cycle attosecond pulses is shown in Fig. 1. Relativistic electrons are generated in a LPWA. The electrons propagate in the z (longitudinal) direction; x and y are the transversal coordinates. The electron beam is propagated through the first triplet of quadrupoles to reduce the divergence of the beam. The length of the nanobunch is proportional to the initial energy spread of the beam. The typical energy spread of a LPWA beam is of a few percent, which does not allow it to generate nanobunches. However, the slice energy spread of the nanobunch can be reduced with a chicane by introducing a phase-space tilt. The process of the slice energy spread reduction was investigated in Ref. [39].

The second triplet of quadrupoles focuses the electron beam to the focus of the THz radiation. In order to generate a spatially periodic energy modulation of the electrons, a high-power laser pulse is superimposed on them in the modulator undulator (MU). This energy modulation leads to the formation of ultrathin (<20 nm) electron layers (nanobunches) in the drift space behind the MU. A counterpropagating strong-field THz pulse is focused to the position where the nanobunch has the smallest longitudinal size and the electrons interact with the THz field.

Advantageously, because of the much easier synchronization, a single laser system is used to drive the attosecond source, including the electron source, the nanobunching, and the THz source. A short-pulse pumped high-power few-cycle optical parametric chirped-pulse amplification (OPCPA) system can be an ideally fitting laser architecture [40–42]. Whereas 10 to 100 TW power OPCPA output pulses are suitable to drive the LPWA and the nanobunching, sub-picosecond to few-picosecond pump pulses can be used to efficiently drive the THz source. Alternatively, even chirped broadband pulses can be used to generate the THz pulses [38].

3. SIMULATION METHODS

The simulation consists of two main parts. First, we estimated the parameters of the accelerated electron beam, generated by a LPWA, and then we calculated the transport and manipulation of the electron bunch, including nanobunch generation. Second, Thomson scattering was calculated with the electron bunch parameters from the first part. In the numerical calculations, in order to reduce the calculation time, macroparticles were considered, rather than individual electrons. Each macroparticle included 2760 electrons.

A. Generation and Manipulation of Relativistic Electrons

In order to create a coherent attosecond source, a good quality electron beam with high charge and few tens of MeV energy is needed. To predict expected electron bunch parameters from a LWFA, we adopted here the scaling law of Gordienko and Pukhov [43]. This law predicted electron bunches with 24 MeV energy and 312 pC charge by focusing few-cycle laser pulses of 8 fs pulse duration and 40 mJ energy to a focal spot diameter of 6 μm. The scaling results were in close agreement with the experiment in Ref. [44].

The coherent attosecond source based on Thomson scattering requires electron bunches of higher charge and energy. Here we assumed 80 mJ laser pulse energy with 800 nm central wavelength, and a pulse duration of 8 fs, corresponding to 10 TW power. The laser pulse was focused in a gas target to an optimized spot size of 3.7 μm corresponding to a peak intensity of 2.9×10^{19} W/cm^2. Following the mentioned scaling law [43], the optimum density for efficient electron acceleration in the bubble regime can be estimated as 1.5×10^{19} cm^{-3} from the condition $n_c(P_0/P) < n_e < n_c(P/P_0)^{1/2}(1/\omega_L\tau)^3$, where n_e is the plasma density, n_c is the critical density, P is the laser power, and $P_0 = m^2c^5/e^2$. An electron beam of 34 MeV energy and 442 pC charge can be obtained in an acceleration distance of 78 μm from the scaling law. The main parameters of the used electron beam are listed in Table 1, which is calculated from the scaling results.

The general particle tracer (GPT) code was used in the calculations to follow the electrons from the electron beam generation to the end of the MU. GPT is based on full 3D particle tracking techniques, enabling the study of 3D and nonlinear effects of charged-particle dynamics in electromagnetic fields [45]. We checked the space charge effect using 10,000

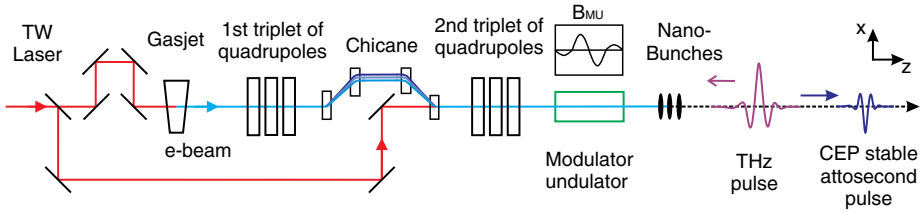

Fig. 1. Scheme of the proposed LPWA-based, THz-driven Thomson scattering setup for single-cycle attosecond pulse generation.

Table 1. Parameters of the Electron Beam from the LPWA

Parameter	Value
Energy (γ_0)	68
Energy spread (σ_{γ_0})	2%
Normalized emittance ($\gamma_0\varepsilon_{x,y}$)	0.078 mm mrad
Transversal size ($\sigma_{x0} = \sigma_{y0}$)	5 μm
Length (σ_{z0})	5 μm
Charge	442 pC

macroparticles and found that this effect is negligible in this charge density (see Fig. 1). In our calculation, 1,000,000 macroparticles were used. Due to the computational limitation, the space charge effect was not taken into account.

The electron beam from a LPWA typically has a large transversal divergence (~1 mrad), the reduction of which is important for further use. Furthermore, it was shown that the generation of coherent radiation is more efficient when the transversal size of the nanobunch is smaller [13]. Therefore, the electron beam was focused by two quadrupole triplets to the THz beam waist. The gradients of the quadrupole triplets were optimized with a self-developed numerical code. In the best case 15 and 25 μm transversal sizes were calculated in the x and y directions, respectively. The first chicane decompresses the electron bunch longitudinally, and after the chicane the slice energy spread of the electron bunch is reduced from 2% to 0.2%. The main parameters of the quadrupoles and the chicane are listed in Table 2.

The relativistic electron beam is sent through the MU, where a 17 TW power laser beam of 800 nm central wavelength is superimposed on it, in order to generate nanobunches. The MU used here has two periods. The magnetic field of the MU is trimmed in antisymmetric design (1/4, −3/4,3/4, −1/4) along the electron propagation direction. The parameters of the modulation process have been summarized in Table 3. After modulating the electron energy with the laser, a series of nanobunches is formed. The individual nanobunches are separated by the modulator laser wavelength. The shortest nanobunch with only 16 nm length, containing a charge of 0.6 pC, was used in the simulation of Thomson scattering. The modulator laser and MU parameters are listed in Table 2. The spatial distribution of the nanobunch is shown in Fig. 2, where the color represents the energies of the macroparticles.

Table 2. Parameters of the Quadrupoles and the Chicane

Parameter	Value
Distance between the gas jet and the first quadrupole triplet	15 cm
First quadrupole triplet gradients	10.1/−7.1/3.2 T/m
First quadrupole triplet elements length	10 cm
Chicane dipole strength	0.043 T
Chicane dipole length	15 cm
Second quadrupole triplet gradients	−2.5/5.6/−6.2 T/m
Second quadrupole triplet elements length	10 cm

Table 3. Parameters of the Modulator Laser and the Modulator Undulator

Parameter	Value
Laser wavelength (λ_l)	800 nm
Laser pulse duration	8 fs
Laser peak power	17 TW
Laser beam waist	1 mm
Laser beam Rayleigh length	3.9 m
MU undulator parameter (K_{MU})	0.5
MU period length (λ_{MU})	6.7 mm

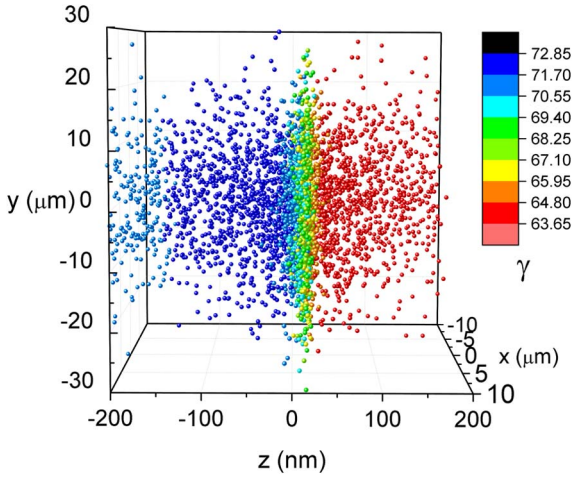

Fig. 2. Spatial and energy distribution of macroparticles in our model. One sphere represents 2760 electrons. The energy distribution of macroparticles (and that of the real electrons) is shown by the color scale.

In the calculation of Thomson scattering, a single nanobunch was considered here. Naturally, the nanobunching process in the proposed setup generates a sequence of nanobunches, rather than one single nanobunch. Consequently, Thomson scattering produces an attosecond pulse train, rather than a single isolated pulse. However, with a nearly single-cycle modulation laser pulse, an isolated nanobunch can be generated [14], allowing for the generation of an isolated single-cycle attosecond pulse by Thomson scattering of a single-cycle THz pulse.

B. Thomson Scattering

The interaction of a thin layer of relativistic electrons with a counterpropagating intense THz pulse results in Thomson scattering, schematically shown in Fig. 3. During the interaction, the electromagnetic field of the THz pulse affects the movement of the electrons according to the Lorentz law. The resulting oscillatory electron motion generates a radiation field, which can be determined based on Lienard–Wiecherd potentials [46] as

$$\vec{E}(\vec{r},t) = \left[\frac{q_e\mu_0}{4\pi}\frac{\vec{R}\times\left((\vec{R}-R\vec{\beta})\times\frac{\mathrm{d}}{\mathrm{d}t}\vec{v}\right)}{(R-\vec{R}\vec{\beta})^3}\right]_{\mathrm{ret}}, \quad (1)$$

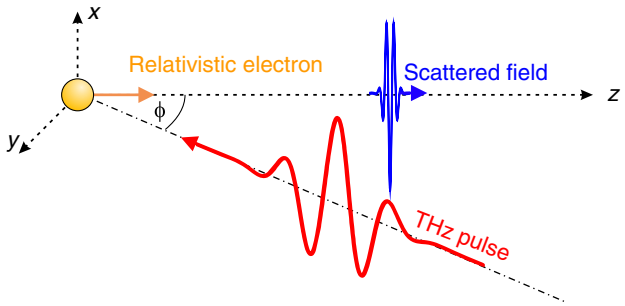

Fig. 3. Scheme of Thomson scattering of a single-cycle THz pulse on relativistic electrons. Both the THz pulse as well as the scattered pulse are polarized along the x direction. The incoming THz pulse propagates in the yz plane.

where q_e is the charge of the electron, μ_0 is the vacuum permeability, $\vec{R}$ is the vector pointing from the position of the electron at the retarded moment to the observation point, $\vec{v}$ is the velocity of the electron, $\vec{\beta} = \vec{v}/c$, and c is the speed of light. Naturally, in case of macroparticles, the charge must be multiplied by the number of electrons in the macroparticle. The energy of the scattered field in the observation plane at $z = z_0$ has been calculated according to Eq. (1) as

$$W = \varepsilon_0 c \iiint E^2(x, y, z = z_0, t)\mathrm{d}t\mathrm{d}x\mathrm{d}y, \tag{2}$$

where ε_0 is the vacuum permittivity [47].

When the THz pulse with λ_0 central wavelength interacts with a relativistic electron, the wavelength of the backscattered radiation field becomes [48]

$$\lambda_r = \frac{1 + a_0^2/2 + \gamma^2\theta^2}{2(1 + \cos\phi)} \cdot \frac{\lambda_0}{\gamma^2}, \tag{3}$$

where $\gamma = (1 - v^2/c^2)^{-1/2}$ is the relativistic factor of the electron, θ is the angle between the electron propagation direction and the observation axis, ϕ is the interaction angle between the THz pulse and the electron, and $a_0 = q_e E_0/m_e c\omega_0$ is the normalized THz field strength, where E_0 is the peak electric field, $\omega_0 = 2\pi c/\lambda_0$ is the angular frequency, and m_e is the mass of the electron.

The scattered field was determined according to Eq. (1), whereby macroparticles, rather than single electrons, were taken into account. Accordingly, q_e and m_e were equal to the charge and the mass of one macroparticle, respectively. In order to use Eq. (1), first it was necessary to solve the equation of motion for the macroparticles in the electromagnetic field of the THz pulse. The equation of motion reads as

$$\frac{\mathrm{d}\vec{p}}{\mathrm{d}t} = q_0(\vec{E}(\rho, z, t) + \vec{v}(t) \times \vec{B}(\rho, z, t)), \tag{4}$$

where $\vec{p} = m_0\gamma\vec{v}$ is the electron momentum vector, m_0 is the mass of the macroparticle, q_0 is the charge of the macroparticle, ρ is the radial coordinate, and t is the time. The electric and the magnetic fields of the THz pulse are given as follows, respectively:

$$\vec{E}(\rho, z, t) = E_0\vec{x}\frac{w_0}{w(z)}\exp\left(-\frac{\rho^2}{w^2(z)}\right) \times \exp\left(-2\ln(2)\frac{(z/c + t)^2}{\tau^2}\right)\cos(k_0(z + ct) - \Psi(z)), \tag{5}$$

$$\vec{B}(\rho, z, t) = \frac{1}{k_0 c}\vec{E}(\rho, z, t) \times \vec{k}_0. \tag{6}$$

In these equations, $\vec{x}$ is the direction of the electric field polarization, w_0 is the THz beam waist radius, $w(z) = w_0\sqrt{1 + (\frac{z}{z_R})^2}$ is the beam radius at position z, $z_R = \frac{\pi w_0^2}{\lambda}$ is the Rayleigh length of the Gaussian beam, λ_0 is the central wavelength of the THz pulse, τ is the full width at half maximum (FWHM) of the intensity in time, $\vec{k}_0 = \frac{2\pi}{\lambda_0}\vec{e}_z$ is the wave vector, and $\Psi(z) = \arctan(\frac{z}{z_R})$ is the Gouy phase. Because single-cycle THz pulses were supposed, the FWHM of the pulses was $\tau = \frac{2\pi}{k_0 c}$.

The energy of the electromagnetic pulse in the vacuum can be calculated according to [47] and Eq. (2), and the field amplitude in Eq. (5) was calculated as

$$E_0 = \frac{2\sqrt{2}(\ln 2)^{\frac{1}{4}}\sqrt{W}}{\sqrt{\epsilon_0 c\pi^{\frac{3}{2}}\tau w_0}}, \tag{7}$$

where ϵ_0 is the vacuum permittivity.

For linear Thomson scattering, the total output radiation yield is proportional to the intensity of the THz pulse [48,49]. Therefore, the THz pulse must be focused to increase its intensity. In the calculations, $w_0 = c/\nu_0$ was assumed, where ν_0 is the central frequency of the THz pulse. Using this focusing and the single-cycle conditions, Eq. (7) gives the following energy- and frequency-dependent relationship:

$$E_0 = \frac{2\sqrt{2}(\ln 2)^{\frac{1}{4}}}{c\sqrt{\epsilon_0 c\pi^{\frac{3}{2}}}}\sqrt{W\nu_0^3}. \tag{8}$$

We note that in the calculations of the next section, head-on collision between the electron and the THz beams was assumed, and Eq. (3) can be simplified to

$$\lambda_r = (1 + a_0^2/2 + \gamma^2\theta^2) \cdot \frac{\lambda_0}{4\gamma^2}. \tag{9}$$

4. RESULTS AND DISCUSSION

We investigated the dependence of the scattered field energy on the frequency and energy of the THz pulse. The results are shown in Fig. 4. In accordance with previous theoretical predictions for laser pulses [48,49], the radiated energy is proportional to the THz pulse energy. Therefore, the scattered radiation energy can be increased by increasing the energy of the THz pulse.

Figure 4 shows that the radiated energy, as a function of the THz frequency, has a maximum at about 0.2 THz. The initial increase at lower THz frequencies can be explained as follows. The number of radiated photons per electron in the case of a

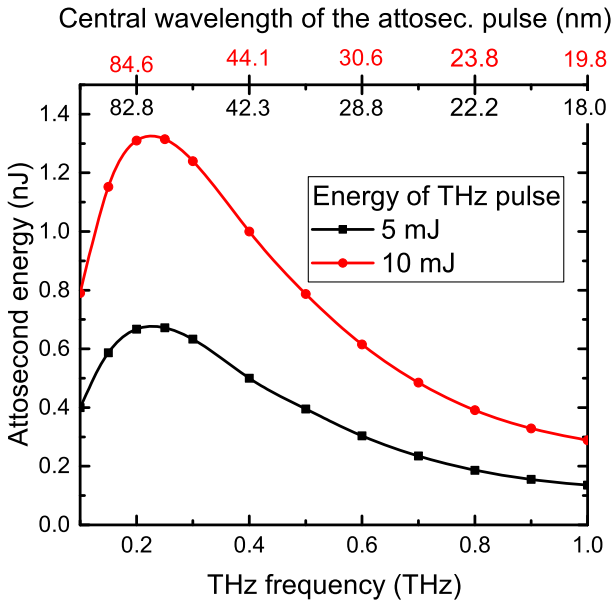

Fig. 4. Energy of the generated single-cycle attosecond pulse as a function of the central frequency of the THz pulse in the case of 5 mJ (black curve) and 10 mJ (red curve) THz pulse energies. The upper axis shows the predicted central wavelength of the emitted radiation according to Eq. (9). Values in black (red) correspond to 5 mJ (10 mJ).

single-cycle THz pulse is given by $N \approx \alpha \cdot a_0^2$ [50], where α is the fine structure constant. The THz pulse energy was kept constant along each curve in Fig. 4, whereby a single-cycle waveform and a diffraction-limited focal spot size was assumed at each value of the THz central frequency. The resulting $a_0^2 \propto W \times \nu_0$ scaling leads to $N \propto \nu_0$. In addition, the energy of the radiated photon also increases with the THz frequency [see Eq. (9)]. This means that the energy emitted by one electron increases with increasing ν_0. As long as transversal effects can be neglected (see below), this leads to an increasing total emitted energy for an extended nanobunch.

However, as the THz frequency, and consequently the radiation frequency, increases, transversal effects for the extended electron sheet become significant. As we showed in [13], owing to coherent superposition, the solid angle of the emitted radiation for a nanobunch with a finite transversal size is smaller than that for a single electron. This also reduces the total radiated energy. Obviously, this effect becomes stronger for higher frequency (smaller wavelength) of the emitted radiation. This is the reason for the decreasing radiated energy with increasing THz frequency.

For a given THz frequency, the energy of the THz pulse is proportional to a_0^2. Therefore, according to Eq. (9), increasing the THz energy at a constant THz frequency results in increasing radiation wavelength as $\lambda_r \propto 1 + a_0^2/2$ for $\theta = 0$. This, together with the $a_0^2 \propto W \times \nu_0$ scaling mentioned above, causes a moderate variation of the radiation wavelength with the THz energy. Increasing the THz energy from 5 to 10 mJ leads to about 2% (10%) shift in the radiation wavelength at 0.1 THz (1 THz) frequency.

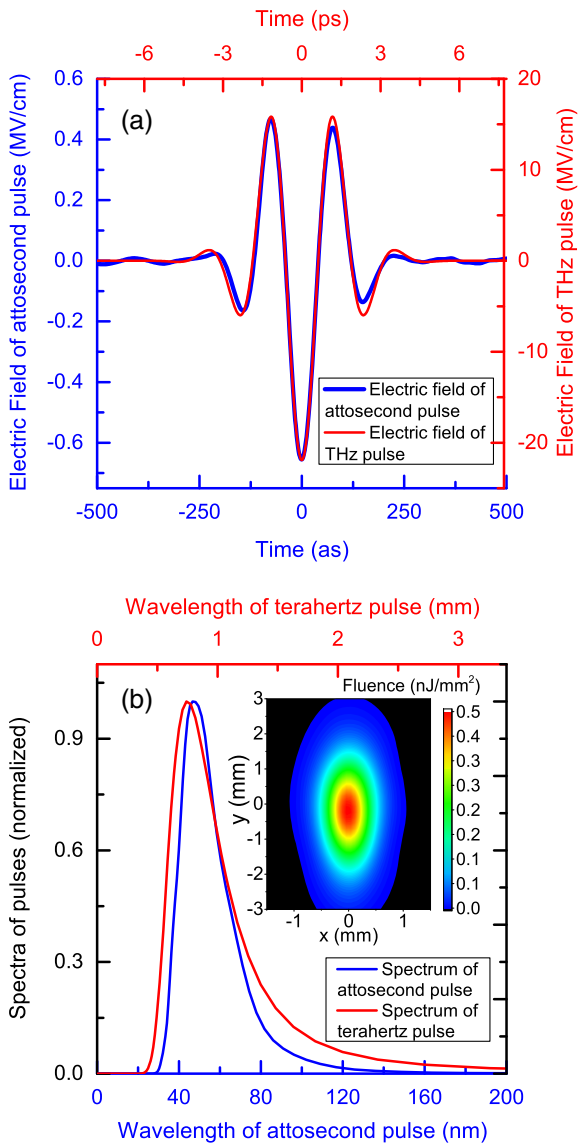

Fig. 5. (a) Temporal waveforms of the Thomson-scattered pulse (blue) and the incoming THz pulse (red). (b) Spectra of the scattered field (blue) and the THz pulse (red). The beam profile of the attosecond pulse on the calculated surface is depicted in the inset.

A comparison of incoming THz and scattered attosecond pulse waveforms and spectra is shown in Figs. 5(a) and 5(b), respectively. In Fig. 5(a) the red curve shows a single-cycle THz pulse with 10 mJ energy and 0.4 THz central frequency. The blue curve shows the scattered field. The two waveforms are very similar. The pulse duration of the scattered pulse is less than 150 as with 48 nm central wavelength, consistent with the single-cycle waveform. The central frequency of the scattered field is about 17,000 times higher than the THz frequency, in good agreement with Eq. (9). This is clearly shown in Fig. 5(b), where the blue curve shows the spectrum of the attosecond pulse and the red curve shows the spectrum of the THz pulse on a 17,000 times larger wavelength scale. Naturally, this similarity between the electric field of the scattered attosecond pulse and the driving THz pulse is maintained for any other

value of the THz carrier-envelope phase and THz frequency, too. The calculated beam profile of the attosecond pulse 50 cm from the focal point of the nanobunch is shown in the Fig. 5(b) inset.

We note that varying the interaction angle ϕ between the propagation direction of the electrons and the propagation direction of the THz pulse (see Fig. 3) allows us to use an electron bunch with still higher energy. For example, $\phi = 90°$ allows for two times larger electron energy to be used. Because the radiated energy is proportional to the square of the electron energy, up to four times higher emitted pulse energy can be expected.

Furthermore, a tunable narrowband extreme ultraviolet source can also be constructed based on the proposed method, whereby a tunable THz source can be used. A suitable THz source can be a semiconductor contact-grating device [33], pumped by the periodically intensity-modulated pulses from a dual-chirped optical parametric amplifier [51].

5. CONCLUSION

A novel scheme of single-cycle attosecond pulse generation was introduced, and investigated by numerical simulations. The entirely laser-based scheme uses electrons of a few tens-of-MeV energy generated by a laser wakefield accelerator, subsequent nanobunching to ultrathin electron layers in a modulating undulator driven by TW laser pulses, and the Thomson scattering of intense THz pulses to generate nanojoule-level attosecond pulses in the few tens of nanometers wavelength range. The scheme can be driven, for example, by a short-pulse pumped few-cycle OPCPA system, whereby strong THz pulses can be conveniently generated by the pump laser. The waveform of the generated attosecond pulses closely resembles that of the THz pulses and can be flexibly shaped by shaping the THz pulse.

Funding. Országos Tudományos Kutatási Alapprogramok (OTKA) (113083); National Research, Development and Innovation Office (125808); Emberi Eroforrások Minisztériuma (EFOP-3.6.2-16-2017-00005); Magyar Tudományos Akadémia; European Union (EFOP-3.6.1.-16-2016-00004).

Acknowledgment. The present scientific contribution is dedicated to the 650th anniversary of the foundation of the University of Pécs, Hungary.

REFERENCES

1. F. Krausz and M. Ivanov, "Attosecond physics," Rev. Mod. Phys. **81**, 163–234 (2009).
2. A. A. Zholents and W. M. Fawley, "Proposal for intense attosecond radiation from an x-ray free-electron laser," Phys. Rev. Lett. **92**, 224801 (2004).
3. E. L. Saldin, E. A. Schneidmiller, and M. V. Yurkov, "Self-amplified spontaneous emission FEL with energy-chirped electron beam and its application for generation of attosecond x-ray pulses," Phys. Rev. ST Accel. Beams **9**, 050702 (2006).
4. A. Marinelli, E. Hemsing, and J. B. Rosenzweig, "Using the relativistic two-stream instability for the generation of soft-x-ray attosecond radiation pulses," Phys. Rev. Lett. **110**, 064804 (2013).
5. D. J. Dunning, B. W. J. McNeil, and N. R. Thompson, "Few-cycle pulse generation in an x-ray free-electron laser," Phys. Rev. Lett. **110**, 104801 (2013).
6. H.-C. Wu, J. Meyer-ter Vehn, B. M. Hegelich, and J. C. Fernández, "Nonlinear coherent Thomson scattering from relativistic electron sheets as a means to produce isolated ultrabright attosecond x-ray pulses," Phys. Rev. ST Accel. Beams **14**, 070702 (2011).
7. A. Paz, S. Kuschel, C. Rödel, M. Schnell, O. Jäckel, M. C. Kaluza, and G. G. Paulus, "Thomson backscattering from laser-generated, relativistically moving high-density electron layers," New J. Phys. **14**, 093018 (2012).
8. W. Luo, H. B. Zhuo, Y. Y. Ma, Y. M. Song, Z. C. Zhu, T. P. Yu, and M. Y. Yu, "Attosecond Thomson-scattering x-ray source driven by laser-based electron acceleration," Appl. Phys. Lett. **103**, 174103 (2013).
9. S. Hack, S. Varró, and A. Czirják, "Carrier-envelope phase controlled isolated attosecond pulses in the nm wavelength range, based on superradiant nonlinear Thomson-backscattering," arXiv:1709.02277 (2017).
10. G. Sansone, E. Benedetti, F. Calegari, C. Vozzi, L. Avaldi, R. Flammini, L. Poletto, P. Villoresi, C. Altucci, R. Velotta, S. Stagira, S. De Silvestri, and M. Nisoli, "Isolated single-cycle attosecond pulses," Science **314**, 443–446 (2006).
11. W. J. Ma, J. H. Bin, H. Y. Wang, M. Yeung, C. Kreuzer, M. Streeter, P. S. Foster, S. Cousens, D. Kiefer, B. Dromey, X. Q. Yan, J. Meyer-ter-Vehn, M. Zepf, and J. Schreiber, "Bright subcycle extreme ultraviolet bursts from a single dense relativistic electron sheet," Phys. Rev. Lett. **113**, 235002 (2014).
12. T. Tanaka, "Proposal to generate an isolated monocycle x-ray pulse by counteracting the slippage effect in free-electron lasers," Phys. Rev. Lett. **114**, 044801 (2015).
13. Z. Tibai, G. Tóth, M. I. Mechler, J. A. Fülöp, G. Almási, and J. Hebling, "Proposal for carrier-envelope-phase stable single-cycle attosecond pulse generation in the extreme-ultraviolet range," Phys. Rev. Lett. **113**, 104801 (2014).
14. Z. Tibai, G. Tóth, Z. Nagy-Csiha, J. A. Fülöp, G. Almási, and J. Hebling, "Investigation of the newly proposed carrier-envelope-phase stable attosecond pulse source," arXiv:1604.08050 (2016).
15. G. Tóth, Z. Tibai, Z. Nagy-Csiha, Z. Márton, G. Almási, and J. Hebling, "Investigation of novel shape-controlled linearly and circularly polarized attosecond pulse sources," Nucl. Instrum. Methods Phys. Res. Sect. B **369**, 2–8 (2016).
16. T. Tajima and J. M. Dawson, "Laser electron accelerator," Phys. Rev. Lett. **43**, 267–270 (1979).
17. S. P. D. Mangles, C. D. Murphy, Z. Najmudin, A. G. R. Thomas, J. L. Collier, A. E. Dangor, E. J. Divall, P. S. Foster, J. G. Gallacher, C. J. Hooker, D. A. Jaroszynski, A. J. Langley, W. B. Mori, P. A. Norreys, F. S. Tsung, R. Viskup, B. R. Walton, and K. Krushelnick, "Monoenergetic beams of relativistic electrons from intense laser-plasma interactions," Nature **431**, 535–538 (2004).
18. C. G. R. Geddes, C. Toth, J. van Tilborg, E. Esarey, C. B. Schroeder, D. Bruhwiler, C. Nieter, J. Cary, and W. P. Leemans, "High-quality electron beams from a laser wakefield accelerator using plasma-channel guiding," Nature **431**, 538–541 (2004).
19. J. Faure, Y. Glinec, A. Pukhov, S. Kiselev, S. Gordienko, E. Lefebvre, J.-P. Rousseau, F. Burgy, and V. Malka, "A laser-plasma accelerator producing monoenergetic electron beams," Nature **431**, 541–544 (2004).
20. V. Malka, J. Faure, Y. A. Gauduel, E. Lefebvre, A. Rousse, and K. T. Phuoc, "Principles and applications of compact laser-plasma accelerators," Nat. Phys. **4**, 447–453 (2008).
21. E. Esarey, C. B. Schroeder, and W. P. Leemans, "Physics of laser-driven plasma-based electron accelerators," Rev. Mod. Phys. **81**, 1229–1285 (2009).
22. X. Wang, R. Zgadzaj, N. Fazel, Z. Li, S. A. Yi, X. Zhang, W. Henderson, Y.-Y. Chang, R. Korzekwa, H.-E. Tsai, C.-H. Pai, H. Quevedo, G. Dyer, E. Gaul, M. Martinez, A. C. Bernstein, T. Borger, M. Spinks, M. Donovan, V. Khudik, G. Shvets, T. Ditmire, and M. C. Downer, "Quasi-monoenergetic laser-plasma acceleration of electrons to 2 GeV," Nat. Commun. **4**, 1988 (2013).
23. S. G. Rykovanov, C. B. Schroeder, E. Esarey, C. G. R. Geddes, and W. P. Leemans, "Plasma undulator based on laser excitation of wakefields in a plasma channel," Phys. Rev. Lett. **114**, 145003 (2015).
24. S. G. Rykovanov, J. W. Wang, V. Y. Kharin, B. Lei, C. B. Schroeder, C. G. R. Geddes, E. Esarey, and W. P. Leemans, "Tunable

polarization plasma channel undulator for narrow bandwidth photon emission," Phys. Rev. Accel. Beams **19**, 090703 (2016).
25. J. W. Wang, C. B. Schroeder, R. Li, M. Zepf, and S. G. Rykovanov, "Plasma channel undulator excited by high-order laser modes," Sci. Rep. **7**, 16884 (2017).
26. M. Vranic, R. A. Fonseca, and L. O. Silva, "Extremely intense laser-based electron acceleration in a plasma channel," Plasma Phys. Controlled Fusion **60**, 034002 (2018).
27. M. E. Couprie, M. Labat, C. Evain, C. Szwaj, S. Bielawski, N. Hubert, C. Benabderrahmane, F. Briquez, L. Chapuis, F. Marteau, M. Valléau, O. Marcouillé, P. Marchand, M. Diop, J. L. Marlats, K. Tavakoli, D. Zerbib, L. Cassinari, F. Bouvet, C. Herbeaux, C. Bourassin-Bouchet, D. Dennetière, F. Polack, A. Lestrade, M. Khojoyan, W. Yang, G. Sharma, P. Morin, and A. Loulergue, "Strategies towards a compact XUV free electron laser adopted for the LUNEX5 project," J. Mod. Opt. **63**, 309–323 (2016).
28. M. C. Hoffmann and J. A. Fülöp, "Intense ultrashort terahertz pulses: generation and applications," J. Phys. D **44**, 083001 (2011).
29. H. Hirori, A. Doi, F. Blanchard, and K. Tanaka, "Single-cycle terahertz pulses with amplitudes exceeding 1 MV/cm generated by optical rectification in $LiNbO_3$," Appl. Phys. Lett. **98**, 091106 (2011).
30. C. Vicario, A. V. Ovchinnikov, S. I. Ashitkov, M. B. Agranat, V. E. Fortov, and C. P. Hauri, "Generation of 0.9-mJ Thz pulses in DSTMS pumped by a $Cr:Mg_2SiO_4$ laser," Appl. Phys. Lett. **98**, 091106 (2011).
31. J. A. Fülöp, Z. Ollmann, C. Lombosi, C. Skrobol, S. Klingebiel, L. Pálfalvi, F. Krausz, S. Karsch, and J. Hebling, "Efficient generation of Thz pulses with 0.4 mJ energy," Opt. Express **22**, 20155–20163 (2014).
32. T. I. Oh, Y. J. Yoo, Y. S. You, and K. Y. Kim, "Generation of strong terahertz fields exceeding 8 MV/cm at 1 kHz and real-time beam profiling," Appl. Phys. Lett. **105**, 041103 (2014).
33. J. A. Fülöp, G. Polónyi, B. Monoszlai, G. Andriukaitis, T. Balciunas, A. Pugzlys, G. Arthur, A. Baltuska, and J. Hebling, "Highly efficient scalable monolithic semiconductor terahertz pulse source," Optica **3**, 1075–1078 (2016).
34. B. K. Ofori-Okai, P. Sivarajah, W. R. Huang, and K. A. Nelson, "Thz generation using a reflective stair-step echelon," Opt. Express **24**, 5057–5068 (2016).
35. L. Pálfalvi, Z. Ollmann, L. Tokodi, and J. Hebling, "Hybrid tilted-pulse-front excitation scheme for efficient generation of high-energy terahertz pulses," Opt. Express **24**, 8156–8169 (2016).
36. L. Pálfalvi, G. Tóth, L. Tokodi, Z. Márton, J. A. Fülöp, G. Almási, and J. Hebling, "Numerical investigation of a scalable setup for efficient terahertz generation using a segmented tilted-pulse-front excitation," Opt. Express **25**, 29560–29573 (2017).
37. C. Vicario, M. Jazbinsek, A. V. Ovchinnikov, O. V. Chefonov, S. I. Ashitkov, M. B. Agranat, and C. P. Hauri, "High efficiency Thz generation in DSTMS, DAST and OH1 pumped by Cr:forsterite laser," Opt. Express **23**, 4573–4580 (2015).
38. X. J. Wu, J. L. Ma, B. L. Zhang, S. S. Chai, Z. J. Fang, C.-Y. Xia, D. Y. Kong, J. G. Wang, H. Liu, C.-Q. Zhu, X. Wang, C.-J. Ruan, and Y.-T. Li, "Highly efficient generation of 0.2 Mj terahertz pulses in lithium niobate at room temperature with sub-50 fs chirped Ti:sapphire laser pulses," Opt. Express **26**, 7107–7116 (2018).
39. M. E. Couprie, A. Loulergue, M. Labat, R. Lehe, and V. Malka, "Towards a free electron laser based on laser plasma accelerators," J. Phys. B **47**, 234001 (2014).
40. J. A. Fülöp, Z. Major, A. Henig, S. Kruber, R. Weingartner, T. Clausnitzer, E.-B. Kley, A. Tünnermann, V. Pervak, A. Apolonski, J. Osterhoff, R. Hörlein, F. Krausz, and S. Karsch, "Short-pulse optical parametric chirped-pulse amplification for the generation of high-power few-cycle pulses," New J. Phys. **9**, 438 (2007).
41. Z. Major, S. A. Trushin, I. Ahmad, M. Siebold, C. Wandt, S. Klingebiel, T.-J. Wang, J. A. Fülöp, A. Henig, S. Kruber, R. Weingartner, A. Popp, J. Osterhoff, R. Hörlein, J. Hein, V. Pervak, A. Apolonski, F. Krausz, and S. Karsch, "Basic concepts and current status of the petawatt field synthesizer—a new approach to ultrahigh field generation," Rev. Laser Eng. **37**, 431–436 (2009).
42. H. Fattahi, H. G. Barros, M. Gorjan, T. Nubbemeyer, B. Alsaif, C. Y. Teisset, M. Schultze, S. Prinz, M. Haefner, M. Ueffing, A. Alismail, L. Vámos, A. Schwarz, O. Pronin, J. Brons, X. T. Geng, G. Arisholm, M. Ciappina, V. S. Yakovlev, D.-E. Kim, A. M. Azzeer, N. Karpowicz, D. Sutter, Z. Major, T. Metzger, and F. Krausz, "Third-generation femtosecond technology," Optica **1**, 45–63 (2014).
43. S. Gordienko and A. Pukhov, "Scalings for ultrarelativistic laser plasmas and quasimonoenergetic electrons," Phys. Plasmas **12**, 043109 (2005).
44. K. Schmid, L. Veisz, F. Tavella, S. Benavides, R. Tautz, D. Herrmann, A. Buck, B. Hidding, A. Marcinkevicius, U. Schramm, M. Geissler, J. Meyer-ter Vehn, D. Habs, and F. Krausz, "Few-cycle laser-driven electron acceleration," Phys. Rev. Lett. **102**, 124801 (2009).
45. http://www.pulsar.nl/gpt.
46. J. D. Jackson, *Classical Electrodynamics* (Wiley, 2007).
47. J.-C. Diels and W. Rudolph, *Ultrashort Laser Pulse Phenomena* (Elsevier, 2006).
48. A. D. Debus, M. Bussmann, M. Siebold, A. Jochmann, U. Schramm, T. E. Cowan, and R. Sauerbrey, "Traveling-wave Thomson scattering and optical undulators for high-yield EUV and x-ray sources," Appl. Phys. B **100**, 61–76 (2010).
49. E. Esarey, S. K. Ride, and P. Sprangle, "Nonlinear Thomson scattering of intense laser pulses from beams and plasmas," Phys. Rev. E **48**, 3003–3021 (1993).
50. S. K. Ride, E. Esarey, and M. Baine, "Thomson scattering of intense lasers from electron beams at arbitrary interaction angles," Phys. Rev. E **52**, 5425–5442 (1995).
51. G. Tóth, J. A. Fülöp, and J. Hebling, "Periodically intensity-modulated pulses by optical parametric amplification for multicycle tunable terahertz pulse generation," Opt. Express **25**, 28258–28272 (2017).